tion, which may affect climate on a global basis.

Gases and particulates may undergo a variety of reactions to produce secondary pollutants that in some cases are more toxic than the parent pollutants. This is particularly true in the case of photochemical smog. Pollutant concentrations are directly related to the density of industry and the use of fossil fuels for power and space heating. Cities that have poor ventilation or frequent temperature inversions are plagued with air pollution episodes.

States have the primary responsibility for atmospheric surveillance. Surveillance systems are usually established on a city or regional basis. The federal monitoring system is to provide a base of uniform data for verification of data from the various agencies and to quantify pollutants that are difficult or expensive to measure.

Presently, the operation of most of the devices and analyzers used for measuring air pollutants is based on wet chemical methods. New techniques are needed in which solid-state or advanced sensing techniques that are based upon the physical or physicochemical properties of pollutants are used. A number of new instruments are presently being developed by NAPCA. In addition, NAPCA has automated and computer-interfaced some of its more sophisticated laboratory and field instrumentation.

Data presented indicate that concentrations of small particulates in the rural or nonurban parts of the country are increasing. Gaseous pollutant concentrations in center-city sites show no particular trend, an indication that downtown areas probably are, and have been for some time, source-saturated.

References and Notes

1. M. O. Amdur, *J. Air Pollut. Contr. Ass.* 19, 638 (1969).
2. "National Emission Reference File," 1970 edition, compiled by A. Hoffman, National Air Pollution Control Administration, Durham, North Carolina.
3. P. M. Wolkonsky, *Arch. Environ. Health* 19, 586 (1969).
4. A. C. Stern, Ed., *Air Pollution* (Academic Press, New York, ed. 2, 1968), vol. 1, p. 30. This work consists of three volumes containing basic resource information on air pollution.
5. T. F. Hatch, in *The Air We Breathe*, S. M. Farber and R. H. C. Wilson, Eds. (Thomas, Springfield, Ill., 1961), p. 115.
6. P. A. Sheppard, *Int. J. Air Pollut.* 1, 31 (1968).
7. "The National Air Pollution Potential Forecast Program" [*Environ. Sci. Serv. Admin. Tech. Mem. WBTM NMC 47* (May 1970)].
8. Averaging times are selected on the basis of data on pollutant effects. Common pollutant averaging times are 1 hour, 2 hours, 8 hours, 24 hours, 1 month, 3 months, and 1 year.
9. Member societies are: Air Pollution Control Association (APCA), American Council of Governmental Industrial Hygienists (ACGIH), American Industrial Hygiene Association (AIHA), American Public Health Association (APHA), American Society of Mechanical Engineers (ASME), American Society for Testing and Materials (ASTM), and Association of Official Analytical Chemists (AOAC).
10. A. E. O'Keefe and G. C. Ortman, *Anal. Chem.* 38, 760 (1966).
11. A. P. Altshuller, personal communication.
12. O. U. Auden, *Anal. Chem.* 41, 428 (1969).
13. B. Henry, personal communication.
14. R. Spirtas and H. J. Levin, "Characteristics of Particulate Patterns, 1957–1966" [*Nat. Air Pollut. Contr. Admin. Publ. No. AP-61* (March 1970)].
15. "Air Quality Criteria for Sulfur Oxides" [*Nat. Air Pollut. Contr. Admin. Publ. No. AP-50* (Jan. 1970)].
16. "Air Quality Criteria for Particulate Matter" [*Nat. Air Pollut. Contr. Admin. Publ. No. AP-49* (Jan. 1969)].
17. "1968 Data Tabulations and Summaries, Continuous Air Monitoring Project, Chicago" [*Air Pollut. Tech. Doc. 69-15* (1969)]; "Continuous Air Monitoring Project, Cincinnati" [*Air Pollut. Tech. Doc. 69-16* (1969)]; "Continuous Air Monitoring Project, Denver" [*Air Pollut. Tech. Doc. 69-17* (1969)]; "Continuous Air Monitoring Project, Philadelphia" [*Air Pollut. Tech. Doc. 69-18* (1969)]; "Continuous Air Monitoring Project, St. Louis" [*Air Pollut. Tech. Doc. 69-19* (1969)]; "Continuous Air Monitoring Project, Washington, D.C." [*Air Pollut. Tech. Doc. 69-20* (1969)].

Earth Strain Measurements with a Laser Interferometer

An 800-meter Michelson interferometer monitors the earth's strain field on the surface of the ground.

Jon Berger and R. H. Lovberg

Geophysicists are interested in the earth's strain field over a very broad band, from frequencies of less than 1 cycle per year to those in excess of hundreds of hertz. Many different geophysical phenomena contribute to this spectrum, but certain strain sources are dominant in particular frequency bands.

At the very lowest frequencies, the cosmologies of Dirac (*1*) and Brans and Dicke (*2*) predict a strain rate of approximately 10^{-10} per year due to the secular decrease in the gravitational constant, which causes an expansion of the earth. From independent geological evidence, other investigators have arrived at the same value (*3*). However, observations of long-term strain rates are very sparse, and, compared with the cosmological or geological time scales, the periods over which they have been made are short. Strain rates of 10^{-5} per year in Japan (*4*), 10^{-6} per year in California (*5*), and 10^{-7} per year in New Jersey (*6*) have been reported. The differences in these rates presumably reflect the varying state of tectonic activity in the respective areas. Seasonal effects such as snow loading, groundwater variations, and thermal expansion are also present in the lower part of the spectrum, but with amplitudes that vary widely with site.

From periods of a week to a few hours, the earth tides dominate the spectrum. These tides are caused by the time-varying perturbations in the earth's gravitational field due to motions of the moon and the sun. The spectrum of earth tides is a line spectrum; the dominant lines are the semidiurnal, with a strain amplitude of 10^{-8}, and the diurnal, with an amplitude of 5×10^{-9}. The literature is replete with observations of earth tides (*7*), since the well-determined nature of the driving source provides a large and ever-present cali-

Both authors are associated with the Institute of Geophysics and Planetary Physics, University of California, San Diego, La Jolla, California 92037. Dr. Berger is a research geophysicist and Dr. Lovberg is a professor of physics.

brated input signal with which to study the earth's response.

Immediately above tidal frequencies, the largest signals are due to the loading of the earth's surface by atmospheric pressure and possibly by the effects of thermal variation on the crust. Because of the scale size of these phenomena, of the order of 10 kilometers, the effects on the strain are quite pronounced.

At frequencies above 1.11 cycles per hour, the lowest resonant frequency of the earth, propagating elastic waves produce strains that dominate the spectrum. The largest signals are produced by earthquakes, but there is always a background level of microseismic activity caused by ocean waves and wind. Typically, the microseismic amplitude is of the order of 10^{-10}, whereas peak dynamic strains from distant earthquakes are often of the order of 10^{-7}.

Techniques of Strain Measurement

When one speaks of earth strain measurements, one is usually referring to measurements of linear extension. Changes in the distance l between two fiducial points are compared with the length l_0 of a standard, and the linear extension or strain is calculated as

$$[\Delta(l - l_0)/l] = \epsilon$$

If it is assumed that the length of the standard l_0 does not change,

$$(\Delta l/l) = \epsilon$$

There are two general classes of techniques for the measurement of earth strain: techniques that actually measure the length l and techniques that only measure relative changes in l. The former include standard surveying techniques, as well as the use of more sophisticated electromagnetic ranging devices. Excellent results have been obtained with these methods in measuring strain rates along the highly active sections of the San Andreas fault system (*8*). However, measurements of this kind are usually neither continuous nor of sufficient sensitivity and stability for many geophysical applications.

The standard instrumental form for the second method of earth strain measurement consists, in essence, of two piers fixed in the ground, with a bar rigidly attached to one pier, extending to within a small distance of the other (*9*). The length standard l_0 is made nearly equal to l, so that $\Delta(l - l_0)$ may be conveniently measured with a variety of electromechanical and optical transducers.

In order to measure earth strain that is representative of the surrounding region, the instrument must be long enough to average out the small-scale

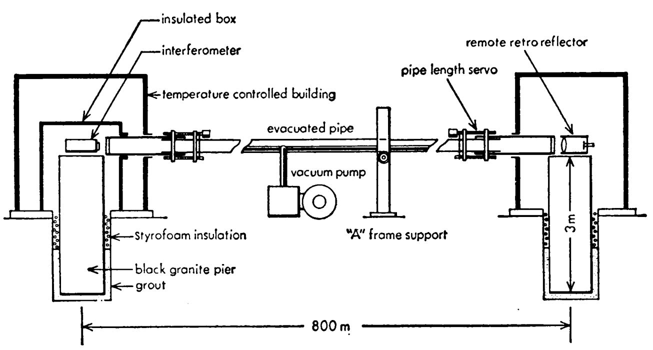

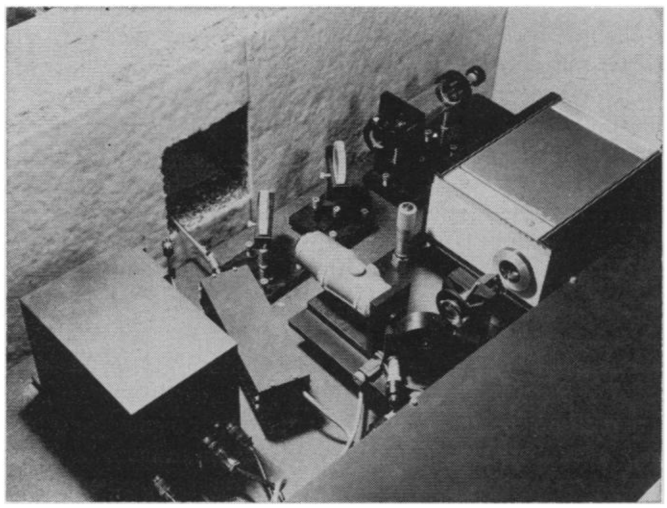

Fig. 1 (above). Mechanical design. Fig. 2 (right). Interferometer encased in insulated box. The laser pictured here is the Spectra Physics model 119. Alternately used is a laser shown schematically in Fig. 4.

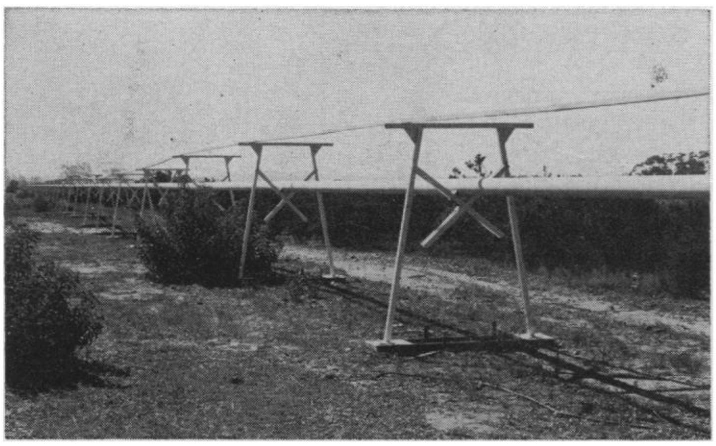

Fig. 3 (above). Evacuated pipe and support systems.

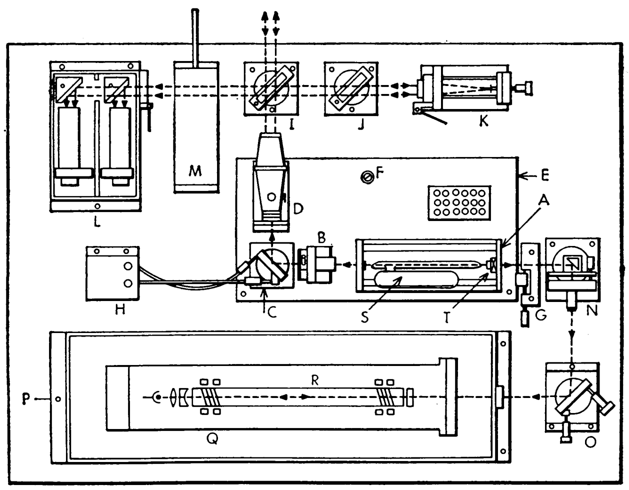

Fig. 4 (right). Schematic of the optical layout of the interferometer. (*A*) Laser resonator structure, (*B*) isolator, (*C*) fine steering mirror, (*D*) beam expanding telescope, (*E*) coarse steering stage, (*F*) coarse vertical micrometer, (*G*) coarse horizontal micrometer, (*H*) right angle drive for fine steering, (*I*) main beam splitter, (*J*) auxiliary beam splitter, (*K*) local retroreflector, (*L*) photomultiplier housing, (*M*) pipe servo sensor, (*N*) steering prism and recollimating lens, (*O*) steering mirror, (*P*) reference cavity stage, (*Q*) reference cavity oven, (*R*) reference cavity, (*S*) plasma tube, (*T*) piezoelectric translator.

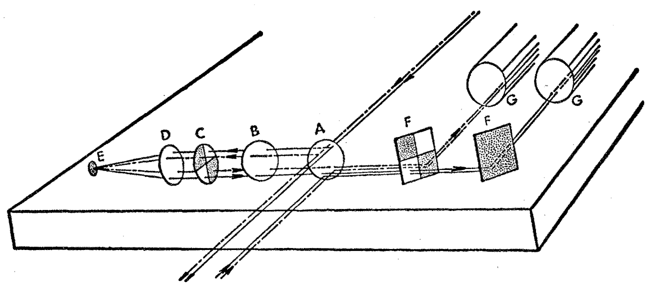

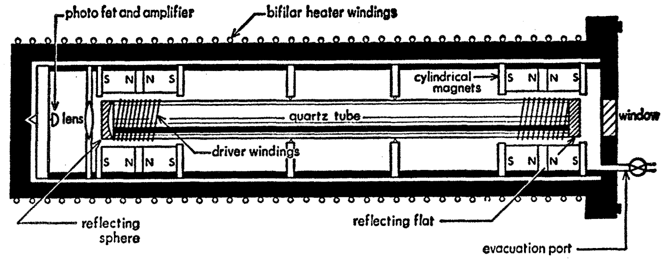

Fig. 5 (left). Phase-shifting optics. (*A*) Main beam splitter, (*B*) auxiliary beam splitter, (*C*) phase shifter, (*D*) retroreflector collimating lens, (*E*) retroreflector mirror, (*F*) quadrant dividing mirrors, (*G*) photomultipliers. Fig. 6 (right). Schematic of the Fabry-Perot reference cavity and oven. The transmitted light is focused by a lens onto a photosensitive field-effect transistor (fet). A thermistor epoxied directly onto the quartz tube monitors the cavity temperature.

inhomogeneities of the rocks on which it rests. Typically, strain meters have a length of the order of 10^2 meters. Problems then arise with the mechanical and thermal stability of the length standard. Quartz (fused silica), which has excellent mechanical properties, has a coefficient of thermal expansion of 5×10^{-7} per degree centigrade. No available material is much better. Hence, to obtain a stability of 10^{-10}, the temperature along the length of the strain meter must be known or be constant to 2×10^{-4} °C. By placing the instruments deep underground in mine shafts or tunnels, reasonably good temperature stability is obtained. However, as measurements extend to lower frequencies, the thermal stability becomes less reliable; hence, the record becomes more noisy. Further, mine shafts and tunnels are not the most desirable sites at which to monitor earth strain. Usually their construction has caused a great deal of fracturing of the rock, and in many mines the geology is by nature inhomogeneous.

Laser Strain Meter

With the development of the laser, it has become possible to extend the techniques of conventional optical interferometry to much greater distances. Interferometers with arm lengths of 1 kilometer have been successfully operated (*10*). A standard Michelson interferometer, with the source and beam splitter on one pier and a reflector on the other, produces a fringe pattern whose motion is indicative of the changes in the distance between the piers, measured in terms of the laser wavelength λ.

The wavelength of a simple laser is not usually a good enough length standard, however. It is determined by a transition line in the lasing gas only to about 1 part in 10^6 for the helium-neon laser, with the exact output wavelength determined by the physical dimensions of the laser optical resonator, the composition of the gas mixture in the plasma tube, and the current density through it. Hence, for the present application, it is necessary to stabilize the laser wavelength by reference to some better external length standard. In effect, then, the laser interferometer is used as an optical comparator, measuring changes in l with reference to some integral multiple of the optical wavelength standard.

There are, in general, two distinct methods by which laser wavelength may be stabilized: by one method the frequency is locked to atomic lines that are particularly sharp or have sharp features; the other method utilizes passive optical resonant cavities. In either case, however, the length standard for the laser strain meter (LSM) can be physically quite small and kept in a well-controlled environment. Hence, it is no longer necessary to use a length standard that is as long as the distance to be measured.

Because of atmospheric refractive index fluctuations, the long optical arm must be evacuated for our purpose. Once the evacuation is accomplished, there are no stringent requirements on thermal stability along the path. It is then feasible to make strain measurements with such an instrument above the surface of the ground. This has the great advantage of obviating the need for a tunnel or mine shaft as an instrument site. Further, in the sense that it may be set up wherever the terrain is fairly level, such an instrument is portable.

Laser interferometers for strain measurements have been built in a variety of optical configurations and lengths (*10–13*). The particular instrument described herein is a second generation LSM developed from the original surface installation described in a previous paper (*11*).

The instrument is presently installed at the University of California's Elliott Field Station, which lies in the northwest corner of Camp Elliott Naval Reservation within the city limits of San Diego, California. The site, being primarily an instrumental proving ground, was chosen for its proximity to the La Jolla campus and not for its particular geophysical interest. It is located at the eastern edge of a broad mesa some 15 kilometers from the Pacific coast. To the east the terrain rises to the Laguna Mountains, which separate the coastal plain from the Anza-Borrego Desert. The highly active San Jacinto fault zone is 50 kilometers east of the site. Immediately to the west is a heavily traveled freeway, and beyond that, some 2 kilometers from the observatory, are the runways of Miramar Naval Air Station.

Mechanical Design

The end piers (Fig. 1), which are the fiducial points of the instrument, are 3-meter-long columns of black granite with a cross section of approximately 1 square meter. Along the lower 1 meter, they are cemented into slightly oversized holes drilled in the rock. The upper part of the columns are free-standing to decouple them from the surrounding layers of the ground. The interferometer chassis and remote retroreflector are mounted directly on the tops of the columns (Fig. 2).

Buildings, heavily insulated thermally and acoustically, enclose both ends, with the interferometer pier further enclosed by a heated box. Temperature control at each end is provided by heat pumps, which maintain the room temperature at $\pm 3°C$, and by a temperature servo control on the box, which keeps that pier temperature constant to $\pm 0.1°C$.

The optical path between the ends is provided by an evacuated stainless steel tube measuring 15 centimeters (outside diameter) by 1.6 millimeters (wall), heliarc-welded at 7.3-meter intervals along its 800-meter length (Fig. 3). The tube is supported on rollers by "A" frames, which allow it to expand and contract freely. It is tied to the ground only at its midpoint. At both ends, servo-controlled expansion joints maintain the distance from pier to tube end to better than 5×10^{-3} centimeter. The tube is evacuated by three large-capacity mechanical pumps to a pressure of 10^{-3} torr.

Optical Design

The light source for the interferometer is a single frequency, unimode, He-Ne laser radiating at a wavelength $\lambda = 6.328 \times 10^{-5}$ centimeter. For long baseline interferometry, it is essential to have a monochromatic source; for convenience, an output in the visible spectrum was chosen, although infrared lasers have been used (*12*). The laser, a Spectra Physics model 119, has a power output of 100 microwatts. The exact output frequency is tunable by the application of a voltage to a piezoelectric translator on which one of the laser cavity mirrors is mounted. This laser is constructed to be highly stable both thermally and mechanically (*14*).

The optical layout of the interferometer is schematically illustrated in Fig. 4. The light from the laser *A* passes through the isolator *B* which serves to decouple the rest of the optical circuit, acting as a "light diode" to prevent light from being reflected back into the laser (*15*). Coarse steering is accomplished by micrometers *G* and *F* which rotate the stage *E* about horizontal and vertical axes. The mirror *C*, gimbal-mounted and driven by micrometers through a compound lever arrangement, provides fine steering adjustment. These micrometers may be controlled from outside the enclosing box by flexible shafts and a right-angle drive unit *H*. The telescope *D* expands the beam from 2 millimeters to 2.5 centimeters and incorporates a spatial filter to re-

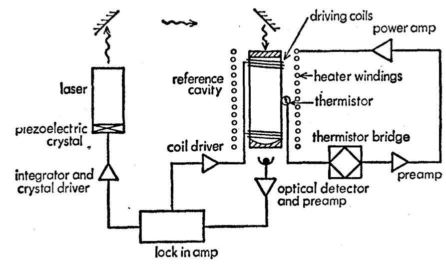

Fig. 7. Stabilizer electronics. The power for the heater windings is provided by an operational amplifier power supply (Kepco model OPS 40-0.5). The integrator and crystal driver are a high-voltage operational amplifier ($\pm$ 150 volts), which controls the frequency response of the servo loop. The overall loop gain is 150 decibels, falling off at 6 decibels per octave from a corner frequency of 5×10^{-6} hertz to a unit gain frequency of 130 hertz.

duce the effects of diffraction spreading from dust particles or other irregularities on elements up to this point in the optical circuit. The light is divided by beam splitter *I*, with half going down the tube to the remote retroreflector and the other half being directed through the auxiliary beam splitter *J* into the local retroreflector *K*. The auxiliary beam splitter compensates for the distortion of beam polarization by the main beam splitter in such a manner that the isolator can be effective for both arms simultaneously (*11*).

The retroreflectors are of the "cat's-eye" type, in which incident rays pass through a converging lens and are reflected from a flat mirror at its focal point. The return rays thus emerge from the lens exactly antiparallel to the entering direction. The use of such retroreflectors in both arms of the interferometer would guarantee, given perfect optics, that (i) the output beam, if successfully steered through the vacuum pipe to the far reflector, will automatically return to the sending point irrespective of substantial pointing errors in the reflector; and (ii) the mixing of the return and reference beams will produce an interference of uniform phase over the whole beam—that is, one will work with the "central fringe."

It has been gratifying that the quality of available optical components has allowed these idealizations actually to be realized. The mirrors in both reflectors are mounted on micrometer screws to allow fine adjustment of focus.

The beam is emitted at a 2.5-centimeter diameter (the radial distribution being a truncated gaussian curve), but it is necessary to provide a larger aperture for the long-arm reflector, since the beam size is somewhat increased by diffraction. With the expanding telescope focused at 800 meters rather than at infinity, one receives at the retroreflector a nearly ideal "bull's-eye" Fraunhofer diffraction pattern, with the first minimum having a diameter of about 5 centimeters. This central 5-centimeter circle is what is actually accepted and returned by the reflector. The truncation here performs a useful spatial filtering of the beam, since the radial intensity distribution of the central spot is itself a good enough approximation to a gaussian curve to allow efficient refocusing to the chassis of the main interferometer, while spurious diffraction features caused by window striae, dirt, or even the initial beam truncation, are eliminated.

To compensate for pressure and temperature variations of the residual air path at the instrument end, the distance from the beam splitter to the mirror of the local retroreflector is made equal to that between the beam splitter and the vacuum tube window. Hence, both paths see equal and compensating variations in air density. The remote retroreflector is placed as close as possible to the tube end and is sealed so that the air inside remains at constant density.

Light from the local retroreflector is mixed with light returning from the remote retroreflector and is passed through a narrow-band interference filter into the detector unit *L*. In order to determine the direction of fringe motion (that is, the relative direction of motion of the two piers), the arrrangement pictured schematically in Fig. 5 is employed. At the entrance to the local retroreflector an element is placed which introduces a phase shift of $\lambda/8$ into each of two opposing quadrants. A ray entering the "cat's-eye" through one of these quadrants always emerges in the opposing quadrant. The net result is that the light from two opposing quadrants is phase-shifted by $\lambda/4$ or 90° with respect to the other two. After recombination with the remote beam, the light enters the photomultiplier housing where, by a system of mirrors, two quadrants are directed into one phototube and two into the other. The phase lead or lag of one photomultiplier signal relative to the other indicates the direction of motion of the piers.

Light from the back end of the laser

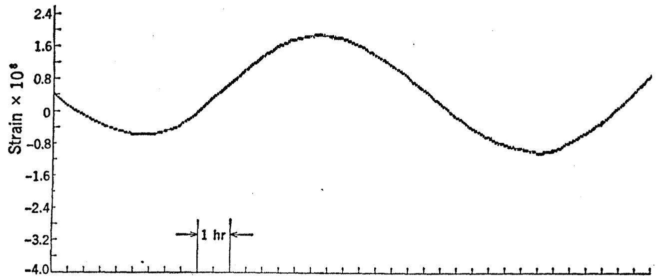

Fig. 8. Raw data sampled at 1 per second. This is the wide-band output containing all frequencies from 0 hertz up to the Nyquist frequency of 0.5 hertz. The steplike nature is a result of the discrete fringe counting, with each step being a strain change of 4×10^{-10}. These data were used to produce the spectra of Figs. 12 and 13.

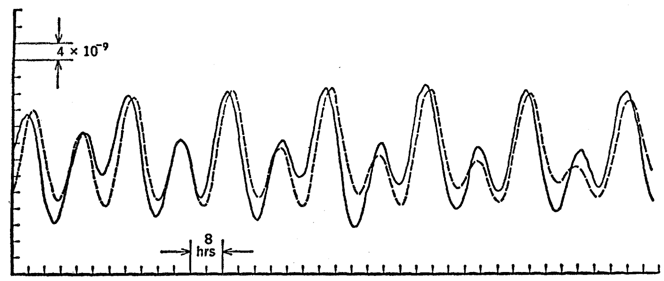

Fig. 9. Data from 10 days of earth tides used in the ocean loading analysis. The solid line is the observed data, recorded at 1 sample per second, low-passed and decimated to 1 sample per 16 seconds. The broken curve is the theoretical strain tide calculated for a yielding earth.

is bent 90° by a steerable prism and recollimated by a lens system mounted in unit *N*. The light is then reflected from the gimbal-mounted mirror *O* into the reference cavity *R*. These two steerable stages allow the entry point and incident angle to be varied independently, so that mode-matching with the cavity can be achieved.

Laser Stabilizer

Stabilized single-frequency lasers are available from several commercial suppliers. Until quite recently, all of these employed the "Lamb dip" scheme of stabilization, in which the laser frequency is locked to the bottom of a slight dip at the center of the optical neon transition line. To generate a signal containing the sign of the frequency error, it is usual to frequency-modulate the laser and to combine the output of an intensity monitor with the modulating signal in a phase detector whose direct-current output corrects the laser frequency. Both the alternating-current modulation and the correction signal are applied to the piezoelectric mount of one of the laser cavity mirrors.

The use of laser frequency modulation causes considerable difficulty in the present application, however. Since the transit time of the light in the long arm is about 5 microseconds, the two components that are mixed at the detector can be substantially different in frequency. Thus the fringe counting circuitry is forced to operate reliably at rates near 1 megahertz merely to keep a correct account of frequency fluctuations. In order to circumvent this difficulty, a stabilizing system has been developed which modulates the frequency of the reference element rather than that of the laser, thus eliminating wavelength "dither," but still allowing the use of an alternating-current, phase-lock servo system.

The reference element is a passive Fabry-Perot optical resonator, consisting of a pair of mirrors held against the lapped ends of an annealed quartz tube of 2.5-centimeter diameter and 30-centimeter length (Fig. 6). One mirror is a flat and the other aspherical section of 3-meter radius. The etalon has a finesse of over 100 and operates in about the millionth order. Thus, a relative frequency shift of 10^{-8} sweeps over an entire resonance of the cavity.

Since the quartz cavity is the frequency standard, it is clear that the entire strain meter can be characterized as a "quartz strain meter." Now, however, the reference rod can be kept in a far more stable environment than would ever be possible in the older type of instrument. The resonator is kept in an oven regulated to about 10^{-4} °C, and, hence, frequency fluctuations attributable to temperature changes are not greater than 10^{-10}. Quartz has another attribute even more important than low thermal expansion, however: so far as we have been able to determine, it is the only commonly available material that has not been observed to "creep"—that is, to exhibit long-term dimensional changes under stress. It is possible to measure and compensate for slight temperature changes, but one is quite helpless against long-term drift in cavity dimensions. Hence, the creep stability has been regarded as the primary figure of merit in resonator material selection.

In order to modulate the reference cavity frequency, the optical path length between mirrors must be changed. Slow scanning systems frequently employ a variation of gas pressure for this purpose. Here, however, it is desirable to operate the servo loop at frequencies that are too high for that technique. One might consider cementing a piezoelectric stack between one mirror and the quartz pipe. This possibility must be rejected, however, since the insertion of cement layers as well as a stack of titanate washers into the support system would certainly vitiate the advantage of the dimensional stability of the quartz.

The procedure finally adopted is to resonate the quartz tube at the frequency of its lowest axial compressional mode, which is 5 kilohertz when the end-loading of the mirrors is taken into account. For this purpose, a pair of

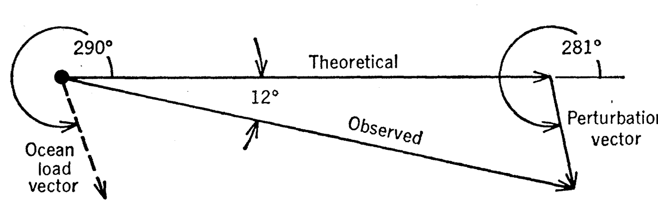

Fig. 10. Tidal phasor diagram for the semidiurnal component of the 10 days of data shown in Fig. 8. The observed and theoretical tides have been identically Fourier-analyzed. The result for the main tidal component (2 cycles per day) is represented as a phasor plot, with the Fourier amplitude at that frequency being the vector magnitude and the Fourier phase angle being the vector phase angle. The theoretical tide component is assigned a magniture of 1 and an angle of 0°. The observed tide component has a magnitude of 1.075 and a phase of −12° (that is, the observed 2-cycle-per-day component leads the theoretical component by 12°). The ocean load vector phase is determined by the phase of the ocean tide and the strain meter orientation. Its magnitude is dependent on the earth model.

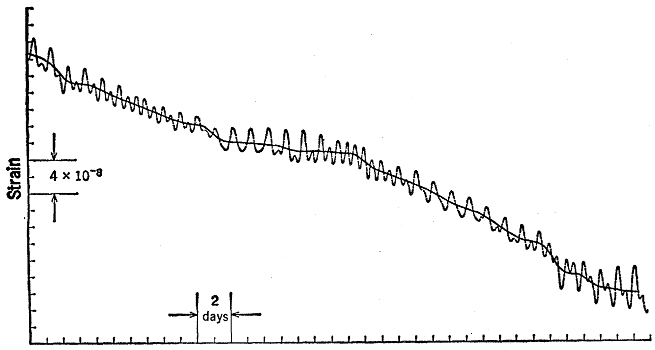

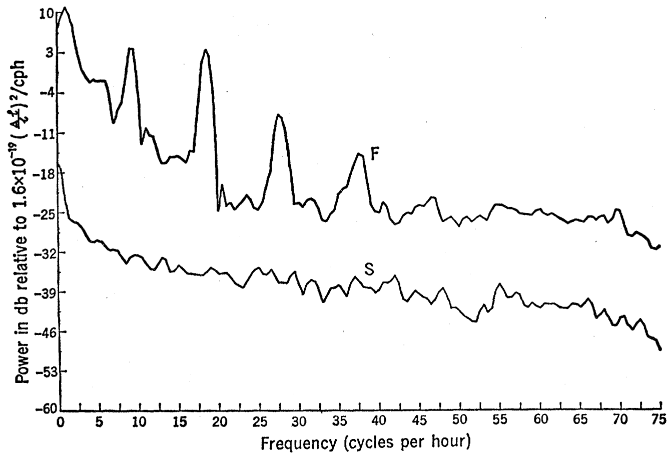

Fig. 11 (above). Data from 42 days of earth tides. The data, recorded at 1 sample per second, were low-pass-filtered and decimated to 1 sample per 16 seconds to produce the broken curve. The solid line was produced by further low-pass-filtering the data to remove the tides. Extension is denoted positive. Fig. 12 (right). Power spectra of the observed strain and the frequency servo-error signal were obtained by analysis of 12.5 hours of simultaneous recording at 1 sample per second. The data were band-pass-filtered to eliminate all frequencies outside the range 0.45 to 72 cycles per hour. The bandwidth for the spectral estimate is 0.5 cycle per hour.

coils, very similar to loudspeaker voice coils, are wound around the quartz tube near its ends, and radial magnetic fields from a pair of external ring magnets are passed through both. A power of less than 1 milliwatt into each coil causes an expansion and shrinkage of the resonator length by about 20 angstroms at a 5-kilohertz rate, which is enough to generate a substantial alternating-current component in the transmission of the cavity. (Each resonance is less than 100 angstroms wide.)

A "lock-in amplifier" (PAR model 120) serves as a scanning frequency generator, phase detector, and amplifier, providing a correction signal to the laser (Fig. 7).

The quartz cavity, together with its mirrors, optical detector, support frame, and magnets, is sealed in a dry argon atmosphere within a heavy aluminum cannister. This container is heated to about 15°C above ambient with the temperature of the can, and the resonator tube itself is monitored by thermistors. A 5-centimeter layer of Styrofoam, surrounded by foil radiation shielding, insulates the assembly.

Fringe Counting

The fringe pattern directed onto the photomultipliers produce signals (*16*)

$$V_x = I_0 + I_1 \cos \frac{4\pi l\epsilon}{\lambda}$$

and

$$V_y = I_0 + I_1 \cos \left[\frac{4\pi l\epsilon}{\lambda} + \phi\right]$$

When the optics are correctly aligned, $\phi = \pi/2$ and the alternating-current signal components are

$$V_x = I_1 \cos \frac{4\pi l\epsilon}{\lambda}$$

and

$$V_y = I_1 \sin \frac{4\pi l\epsilon}{\lambda}$$

Then

$$V_x^2 + V_y^2 = I_1^2$$

and

$$\tan\theta = \frac{V_y}{V_x} = \tan\frac{4\pi l\epsilon}{\lambda}$$

If these two signals are applied to the x and y inputs of an oscilloscope, the resulting pattern will be a spot moving around the circumference of a circle of radius I_1, with an angular position θ which is related to the instantaneous value of the strain ϵ by:

$$\epsilon = \frac{\lambda}{4\pi l} \arctan \frac{V_y}{V_x}$$

Each revolution of the spot corresponds to the passage of one fringe or a strain change of

$$\epsilon = \frac{\lambda}{2l} = 4 \times 10^{-10}$$

The data presented later in the article were obtained with a counting system that produced 1 count for every full fringe (*11*). The least count strain was thus 4×10^{-10}. The counting system currently under development produces a count for every one-fourth fringe of motion (that is for every 90° rotation of the spot). Thus, there are 4 counts per fringe and the least count strain is 10^{-10}.

In principle, the sensitivity of this instrument may be greatly increased by the addition of an analog device, which locks onto a single fringe and produces an output proportional to θ. Several devices have been suggested and constructed (*10, 17*). Ultimately, of course, uncertainties in laser frequency will vitiate this sensitivity by producing more noise than signal. At the present site of our instrument, "cultural" noise, in particular jet engine noise from the nearby airfield, limits the useful sensitivity to about 1 part in 10^{10}. A quieter site might allow an increase in sensitivity by an order of magnitude or more. The stability or long-period noise is controlled by the stability of the reference length. Laser frequency stabilization schemes such as described here probably provide 1 part in 10^{10} relative stability over long periods of time. A new system of stabilization (*12*), where the laser frequency is locked to an atomic standard, promises stability as much as two orders of magnitude greater than we have achieved with the present technique.

Results

The output from the fringe counter is recorded on digital magnetic tape at a standard rate of 1 sample per second (Fig. 8). During special events such as announced nuclear bomb tests, the sample rate may be increased to 146 samples per second. In addition, there is an analog output on a strip-chart recorder.

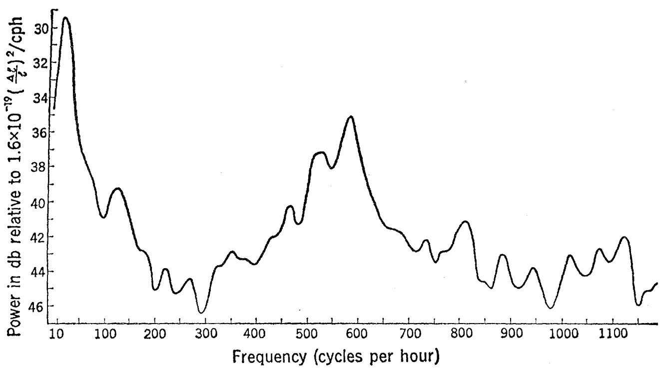

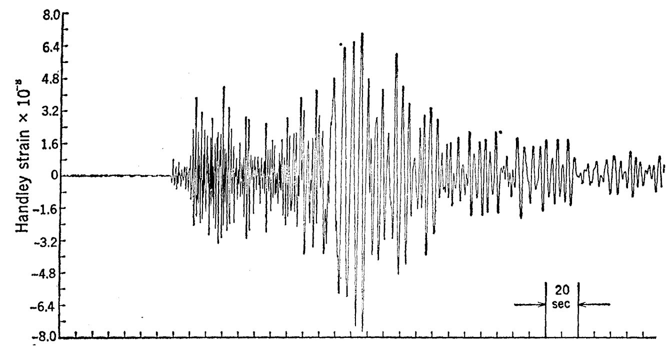

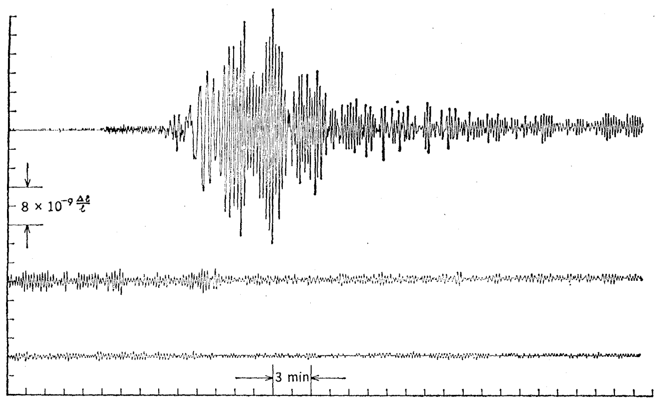

Fig. 13 (left above). Power spectrum of observed strain showing the microseismic peak. One hour of data was low-pass-filtered to remove frequencies below 20 cycles per hour. The spectral estimate has a bandwidth of 10 cycles per hour.

Fig. 14 (right above). First part of strain record from the 1-megaton nuclear test "Handley," detonated at the Nevada Test Site on 26 March 1970. The U.S. Coast and Geodetic Survey magnitude is $M_B = 6.5$; $M_s = 5.3$.

Fig. 15 (left below). The strain record from an earthquake just offshore in the Pacific near the Mexico-Guatemala border, 29 April 1970. The epicentral distance is 3200 kilometers, and the great circle path from the epicenter makes an angle of 81° with the axis of the strain meter. The magnitude reported by the U.S. Coast and Geodetic Survey is $M_s = 7.3$. The origin time is the beginning of the plot, and the lower two traces are continuations of the record.

The counting electronics have been constructed to have a bandwidth of 1 megahertz. Hence, the counter will follow motions up to 10^6 fringes per second. This corresponds to a rate of strain of 10^{-4} per second for the 4-count-per-fringe system, or a relative velocity of the piers of 8 centimeters per second. The instrument response is flat over the frequency band $0 < f < 10^6$ hertz and introduces neither amplitude changes nor phase shifts. Further, it is linear over the entire dynamic range which extends from relative pier motions of one-fourth fringe or 1.5×10^{-5} centimeter to several centimeters (the distance from the end of the evacuated tube to the remote retroreflector).

It is important to emphasize that, even though the strain least count is 10^{-10}, phenomena with smaller amplitude may be detected by averaging the recorded output. The process of fringe counting is a form of amplitude quantization and introduces an uncertainty similar to digitization in the time domain. This uncertainty may be expressed as a noise power level below which signals have a signal-to-noise ratio of less than 1. For a recording rate of 1 sample per second, this least count noise is 2.5×10^{-25} $(\Delta l/l)^2$ per cycle per hour (− 58 decibels on the scale of Figs. 12 and 13).

One of the problems in the measurement of long-period earth strain is the verification that the data are not contaminated by instrumental noise. Individual calibrations of various parts of the instrument are, of course, possible, but what is needed is an overall system calibration that includes the instrument-earth interface. Fortunately, nature provides a convenient calibrating signal in the form of the earth tides. From a knowledge of the earth-moon astronomy and the earth structure (obtained mostly from seismology), the input signal is known to a few percent. However, in the analysis of earth tide data from stations near an ocean, the effects of the ocean load on the earth's crust must be taken into account. The Elliot Field Station, being only 15 kilometers from the edge of the Pacific, will be strongly subject to such effects. In Fig. 9 a 10-day record of earth tides is plotted with the theoretical strain tide on a yielding earth (*15*). Slight amplitude and significant phase differences are immediately obvious. The semidiurnal component of the tide may be represented [following Farrell (*18*)] in a phasor diagram (see Fig. 10).

The tides along the Pacific coast of North America have been analyzed in some detail by Munk *et al.* (*19*). They find that, for the semidiurnal component, the observations may be mostly explained by supposing that the tide is a southward propagating wave, which is trigonometric along the shore and dies off exponentially seaward. The phase of the ocean load vector is then simply related to the phase of the ocean tides and the orientation of the strain meter. The observed perturbation vector phase of 281° agrees with the ocean load phase of 290° to within the accuracy of the knowledge of the offshore ocean tides. The magnitude of the load vector is dependent upon the earth model. For a simple, flat, homogeneous earth, the two vectors have equal magnitude when the mean effective rigidity is 1.7×10^{12} dynes per square centimeter, the rigidity of the earth at a depth of approximately 800 kilometers. It is not particularly instructive to refine this calculation, since the present knowledge of the offshore ocean tides is rather imprecise. However, the agreement obtained between the observed earth tides and the theoretical input lends credence to the long-period strain observations. Further, by using the detailed earth models derived from seismology, the problem may be inverted and the observed earth tides used to study the deep ocean tides (*20*).

Since strain observations were first obtained with the original LSM in November 1968, the record has consistently shown ground compression at subtidal frequencies. Figure 11 shows a 42-day run of strain data. The average linear strain rate over this period was 7.7×10^{-9} per day. This rate (averaged over 5-day periods) has varied from 10^{-10} to 2×10^{-8} per day but has never reversed sign.

The magnitude and persistence of the effect make it difficult to account for these observations in terms of instrumental drift. Moreover, the present instrument produces the same results as did the orginal. There seems to be no significant seasonal variation of the strain rate nor any obvious correlation with local conditions. Hence, we conclude that these high strain rates may be associated with regional tectonic activity.

Figure 12 shows power spectra of the earth strain and of the frequency servo-error signal over the band in which the free oscillations of the earth are observed. The frequency servo-error signal is the signal that is applied to the piezoelectric translator in the laser cavity in order to lock the laser frequency to the resonant frequency of the reference cavity. Its spectrum is expressed in equivalent strain units; it represents the earth strain spectrum that would be inferred if the laser were unstabilized. The need for a frequency stabilizer is obvious. The peaks in this spectrum are caused by the temperature cycling of the heat exchangers in the instrument house. In general, the servo-error signal falls off at 6 decibels per octave (that is, like $1/f^2$ in amplitude), whereas the spectrum of the earth strain falls off at about half that rate, or 3 decibels per octave (that is, like $1/f$ in amplitude).

The spectrum peaks again, owing to microseismic activity, at about 600 cycles per hour (that is, 6-second period) (Fig. 13). Even though the root-mean-square amplitude of the earth strain over the microseismic band is often 10^{-1} of a least count and cannot be seen on the time-domain record, the peak in the spectrum is quite clear.

Figure 14 shows the wide-band output during the 1-megaton nuclear test "Handley," exploded at the Nevada Test Site on 26 March 1970. Digital recordings at a rate of 8 samples per second taken during announced nuclear tests yield distortionless strain spectra from 0 to 4 hertz. Such recordings allow resolution of the rise time of the first arrival and a highly sensitive indication of any zero frequency strain offsets that may occur.

Earthquakes (Fig. 15) are recorded at the standard sample rate of 1 sample per second.

Summary

The development of the laser as a source of coherent optical radiation has permitted the application of interferometric techniques to the problem of earth strain measurement. By use of this technology, an 800-meter laser strain meter has been developed which operates above the surface of the ground. The instrument has a strain least count of 10^{-10}, requires no calibration, and has a flat and linear response from zero frequency to 1 megahertz. The linearity and large dynamic range of the laser strain meter offer unprecedented versatility in the recording of seismic strains associated with earthquakes and nuclear blasts. The extremely wide bandwidth opens new areas of the strain spectrum to investigation.

A key to the understanding of the state of stress of the earth and the association phenomona of tectonic activity and earthquakes is a knowledge of the spatial distribution of the earth strain. Measurements of secular strain and earth tides indicate that, even at these long periods, surface strain measurements are valid representations of earth strain at depth. The LSM thus provides a means of making crustal strain measurements at points selected for maximum geophysical interest and ultimately allows the mapping of strain field distributions.

References and Notes

1. P. A. M. Dirac, *Proc. Roy. Soc. Ser. A* **165**, 199 (1938).
2. C. Brans and R. H. Dicke, *Phys. Rev.* **124**, 425 (1961).
3. K. M. Creer, in *Dictionary of Geophysics* (Pergamon, Oxford, 1967), vol. 1, p. 383.
4. M. Takada, *Third International Symposium on Earth Tides of the International Association of Geodesy* (Istituto di Topografia e Geodesia dell'Università Trieste, Trieste, 1959), p. 127.
5. C. H. Scholz and T. S. Fitch, *J. Geophys. Res.* **74**, 6649 (1969).
6. M. W. Major, G. H. Sutton, J. Oliver, R. Metsger, *Bull. Seismol. Soc. Amer.* **54**, 295 (1964).
7. P. Melchior, *The Earth Tides* (Pergamon, Oxford, 1966).
8. R. B. Hofmann, *Calif. Dep. Water Resour. Bull. 116-6* (May 1968).
9. H. Benioff, *Bull. Seismol. Soc. Amer.* **25**, 283 (1935).
10. V. Vali and R. C. Bostrom, *Rev. Sci. Instrum.* **39**, 1304 (1968).
11. J. Berger and R. H. Lovberg, *ibid.* **40**, 1569 (1969).
12. H. S. Boyne *et al.*, in *Laser Applications in the Geosciences* (Western Periodicals, North Hollywood, Calif., 1970), p. 215.
13. G. C. P. King and D. Davies, *The Application of Modern Physics to the Earth and Planetary Interiors* (Wiley, London, 1969), p. 513.
14. Under development, and shown in the optical circuit schematic (Fig. 3), is a laser that has the properties mentioned above but in addition is constructed in such a manner that the plasma tube may be quickly replaced without disturbing the resonator structure. This feature speeds the laser replacement time considerably, since no realignment of the optics is necessary.
15. J. Berger, thesis, University of California, San Diego (1970).
16. In the equations that follow, V_x and V_y are the two photomultiplier outputs, I_0 is the voltage offset resulting from the average light intensity, I_1 is the modulation amplitude of the fringes, l is the long arm length, λ is the laser wavelength, and ϵ is the strain.
17. J. Berger, in *Laser Applications in the Geosciences* (Western Periodicals, North Hollywood, Calif., 1970), p. 203.
18. W. E. Farrell, thesis, University of California, San Diego (1970).
19. W. Munk, F. Snodgrass, M. Wimbush, *Geophys. Fluid Dyn.* **1**, 161 (1970).
20. W. E. Farrell, *Symp. Int. sur Les Marees Terrestres, 6th* (Strasbourg, 1969).
21. We thank F. Wyatt who assisted in the design and construction of the instrument described here. The work was supported by the Environmental Science Services Administration grant E-22-2-70(G) and by the Advanced Research Project Agency of the Department of Defense, monitored by the United States Army Research Office—Durham under contract DA-31-124-ARO-D-257.